



This is a repository copy of *Metal-organic nanosheet gels: Hierarchically porous materials for selective loading and differential release*.

White Rose Research Online URL for this paper:

<https://eprints.whiterose.ac.uk/229141/>

Version: Published Version

---

**Article:**

Tan, J. and Foster, J.A. [orcid.org/0000-0002-0588-2474](https://orcid.org/0000-0002-0588-2474) (2025) Metal-organic nanosheet gels: Hierarchically porous materials for selective loading and differential release. *Advanced Functional Materials*. e07474. ISSN 1616-301X

<https://doi.org/10.1002/adfm.202507474>

---

**Reuse**

This article is distributed under the terms of the Creative Commons Attribution (CC BY) licence. This licence allows you to distribute, remix, tweak, and build upon the work, even commercially, as long as you credit the authors for the original work. More information and the full terms of the licence here:

<https://creativecommons.org/licenses/>

**Takedown**

If you consider content in White Rose Research Online to be in breach of UK law, please notify us by emailing [eprints@whiterose.ac.uk](mailto:eprints@whiterose.ac.uk) including the URL of the record and the reason for the withdrawal request.



[eprints@whiterose.ac.uk](mailto:eprints@whiterose.ac.uk)  
<https://eprints.whiterose.ac.uk/>

# Metal-Organic Nanosheet Gels: Hierarchically Porous Materials for Selective Loading and Differential Release

Jiangtian Tan\* and Jonathan A. Foster\*

Metal-organic nanosheets (MONs) are intrinsically porous 2D materials with a high surface area and tunable chemistry, which have been widely used in suspensions or on surfaces for a variety of applications. Here, this work demonstrates that MONs can be used to form gels through a simple centrifugation process, and their hierarchically porous structures used to enable the selective loading and differential release of small molecules based on their size and charge. Centrifugation of a suspension of monolayer Zr-BTB MONs (BTB = 1,3,5-benzenetribenzoate) formed gels in a range of solvents with a concentration of  $\approx 1.5$  wt.%. The gels displayed rapid self-healing behavior, can be extruded through a syringe needle into different shapes, and freeze-dried to form self-supporting aerogels. Rapid and selective loading of the gels with a range of small molecules can be achieved by centrifugation of suspensions of nanosheets containing different cargo solutions. Small neutral molecules are found to diffuse out of the gel significantly faster than larger molecules, which is attributed to the nanosheets acting as “fishing nets” that allow small molecules to pass through the pores, whilst larger molecules have to take a tortuous path through the hierarchically porous structure. Charged molecules are released slower than the neutral ones, which is attributed to electrostatic interactions with the nanosheets. It is anticipated that hierarchically porous MON-based gels will open up a variety of interesting new applications, including sensing, separation, controlled release, drug loading, and drug delivery.

in which growing 3D metal-organic framework (MOF) crystals fuse with each other to form a sample spanning network.<sup>[4]</sup> Other examples combine MOFs with gel forming polymers,<sup>[5]</sup> or use crosslinkers to chemically or physically cross-link MOFs followed by removing metal ions.<sup>[6,7]</sup> A variety of MOG derived materials have also been developed in which the MOGs act as sacrificial templates to create porous gel-derived materials.<sup>[8,9]</sup> The solvent containing macro-pores of the gel, combined with the inherent microporosity of the MOFs gives MOGs a unique hierarchical structure.<sup>[2]</sup> Porous materials are important for a wide range of advanced separation applications<sup>[10–12]</sup> and MOGs have been harnessed in applications ranging from removing dyes from water,<sup>[13]</sup> to separating enantiomers.<sup>[14]</sup> Solution processability is another key advantage of MOGs over traditional microcrystalline MOF powders. For example, Somjit and co-workers studied UiO-66 MOG, and showed that it can be processed into a thin film with sub-100 nm thickness via spin-coating, which enhanced the electrical conductivity of their devices.<sup>[15]</sup> A variety of

other MOGs, such as HKUST-1, UiO-66-NH<sub>2</sub>, have been processed into monolithic materials and have shown great promise for gas uptake applications.<sup>[16–18]</sup> A wide variety of other porous materials have also been adapted to form gels and aerogels, including metal-organic polyhedra,<sup>[19–21]</sup> and porous polymers.<sup>[22,23]</sup>

Metal-organic nanosheets (MONs) are 2D MOFs with a sheet-like morphology.<sup>[24]</sup> Their ultrathin nature, high aspect ratios, and high surface areas make them ideal materials for a wide range of applications, including sensing, catalysis, and electronics.<sup>[25]</sup> Moreover, their varied and well-defined pore size, shape, and chemistry make them ideal materials for use in water-purification and gas separation applications.<sup>[26,27]</sup> Among the diverse range of MONs that have been reported in the literature, Zr-BTB MONs (BTB = 1,3,5-benzenetribenzoate) have attracted considerable attention due to their high water, chemical and thermal stability, ease of synthesis and functionalization,<sup>[1,28,29]</sup> which have been used in a wide range of different applications including catalysis, sensing and separation.<sup>[30–34]</sup>

Inorganic 2D materials, most notably clays and graphene oxide, are well known to form gels.<sup>[35–38]</sup> The gels have been used extensively in a wide range of biomedical,<sup>[39]</sup> environmental<sup>[40]</sup>

## 1. Introduction

Metal-organic gels (MOGs) have attracted considerable attention thanks to their highly tunable structures and intrinsic porosity.<sup>[2,3]</sup> Most MOGs are formed through a sol-gel process

J. Tan  
Centre for Molecular Systems and Organic Devices (CMSOD)  
State Key Laboratory of Flexible Electronics (LoFE) & Institute of  
Advanced Materials (IAM)  
Nanjing University of Posts & Telecommunications  
9 Wenyuan Road, Nanjing 210023, China  
E-mail: 1163889729@qq.com

J. A. Foster  
School of Mathematical and Physical, Sciences  
The University of Sheffield  
Sheffield S3 7HF, UK  
E-mail: jona.foster@sheffield.ac.uk

© 2025 The Author(s). Advanced Functional Materials published by Wiley-VCH GmbH. This is an open access article under the terms of the Creative Commons Attribution License, which permits use, distribution and reproduction in any medium, provided the original work is properly cited.

DOI: 10.1002/adfm.202507474

and energy applications.<sup>[41]</sup> In these gels the nanosheets form sample spanning networks through either electrostatic interactions or chemical cross-linking by polymers or metal ions.<sup>[35,42,43]</sup> To our knowledge, there are no examples of MONs being harnessed in the gel state for use in any applications. We are aware of only one mention of MONs forming gels in the literature, a study by Zhao and co-workers, where they observe Zr-BTB showing gel-like behavior during the formation of thin films, which they were developing for capacitive gas sensing.<sup>[29]</sup>

In this work, we report a new approach to the formation of MOGs through centrifugation of suspensions of 2D MONs. We characterize the rheology and structure of the gels for the first time and discover self-healing behavior and aerogel formation. We hypothesised that the high surface area and porosity of the nanosheets and gels could make them interesting candidates for small molecule cargo loading and release applications. In particular, we envisaged the microporous, sheet-like MONs acting as “fishing nets” with small molecule “fish” being able to pass through the pores, whereas larger molecules are blocked by the pores, and charged molecules stick to the MONs. We anticipated that this could enable size- and charge-selective loading and differential release of cargo molecules from MON-based gels, opening up new levels of control for capture and release applications.

## 2. Results and Discussion

### 2.1. Preparation and Characterization of Zr-BTB MONs

Zr-BTB MONs were synthesized according to the solvothermal method reported by Zhao and co-workers.<sup>[29]</sup> As shown in **Figure 1a**, zirconium(IV) chloride ( $\text{ZrCl}_4$ , 0.129 mmol) and 1,3,5-benzenetribenzoic acid ( $\text{H}_3\text{BTB}$ , 0.068 mmol) were dissolved in a mixture of formic acid ( $\text{HCOOH}$ , 2 mL), water ( $\text{H}_2\text{O}$ , 2 mL), and *N,N*-dimethylformamide (DMF, 15 mL). The reaction mixture was heated in a reaction oven at 120 °C for 24 h. The resulting viscous suspension of Zr-BTB MONs was then centrifuged and washed three times with fresh DMF then ethanol. The washed MONs were stored in fresh ethanol as a homogeneous suspension with a concentration of 2.5 mg mL<sup>-1</sup> until needed.

The ethanol suspension of Zr-BTB MONs (1 mL) was dried using a hot plate at 80 °C to remove most of the solvent, followed by complete drying at 120 °C. The dried solids were characterized by powder X-ray diffraction (PXRD). The PXRD pattern of the as-synthesized Zr-BTB MONs (**Figure S1**, Supporting Information) was consistent with that reported by Zhao and co-workers,<sup>29</sup> suggesting that phase-pure materials were synthesized. Whereas, compared to the simulated PXRD pattern of 3D Zr-BTB, the as-synthesized Zr-BTB MONs showed a significantly reduced number of peaks. This could be attributed to the extreme aspect ratio of the nanosheets, resulting in line broadening and preferred orientation effects (**Figure S1**, Supporting Information). The Brunauer–Emmett–Teller (BET) surface area of Zr-BTB MONs was calculated to be 360 m<sup>2</sup> g<sup>-1</sup> (**Figure S2**, Supporting Information), which was consistent with the surface area reported in the literature.<sup>[29]</sup>

Scanning electron microscopy (SEM) characterization of the Zr-BTB MONs showed their 2D sheet-like morphology (**Figure S3**, Supporting Information), and dynamic light scattering (DLS) characterization showed that the particle size of the Zr-BTB

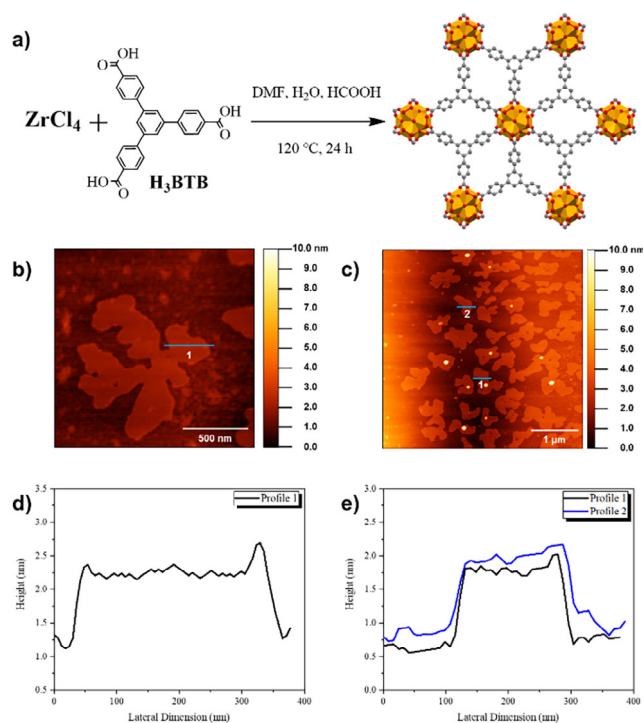


**Figure 1.** a) Synthesis of Zr-BTB MONs. The crystal structure of Zr-BTB was downloaded from CCDC (deposition number: 1567188). b–e) AFM images and associated height profiles of Zr-BTB MONs.

MONs was in the range of 1.4 μm–6.5 μm (**Figure S4**, Supporting Information). Atomic force microscopy (AFM) characterizations showed that the thickness of Zr-BTB MONs was ≈1.5 nm, which was comparable to the van der Waals sizes of  $\text{Zr}_6$  clusters in Zr-BTB (1.2 nm),<sup>[34]</sup> confirming the formation of monolayer nanosheets (**Figure 1b–e**). It is worth noting that the Zr-BTB MONs prepared in this work were thinner than the 13 nm thick Zr-BTB nanosheets reported by Zhao and co-workers,<sup>[29]</sup> but comparable to the 1.2 nm thick Zr-BTB nanosheets reported by Lin and co-workers.<sup>[34]</sup>

### 2.2. Preparation and Characterization of Gels

Whilst attempting to isolate Zr-BTB nanosheets from a suspension of ethanol by centrifugation, we noticed that around one fifth of the solvent at the bottom of the centrifuge tube was immobilized by the nanosheets. The resulting material was stable with respect to inversion (**Figure 2a**), a crude but widely used method for identifying gel formation.<sup>[3,44–46]</sup> In a typical experiment, 25 mg of Zr-BTB was dispersed in 10 mL of ethanol by shaking and centrifuged at 4500 rpm for 1 h. Approximately 2 mL of gel was isolated with the other 8 mL of ethanol carefully removed using a pipette. Drying of the ethanol gel confirmed that it contained 1.5 wt.% of MONs by mass. Gel formation was observed in a wide range of other organic solvents including acetone, DMF, chloroform, tetrahydrofuran (THF), pentane, and toluene as well as deionized (DI) water with 1.5–2.5 mL of solvent immobilized by 25 mg of MONs (**Figure 2a**; **Table S2**, Supporting Information). In all cases except DI water, stable gels were formed after

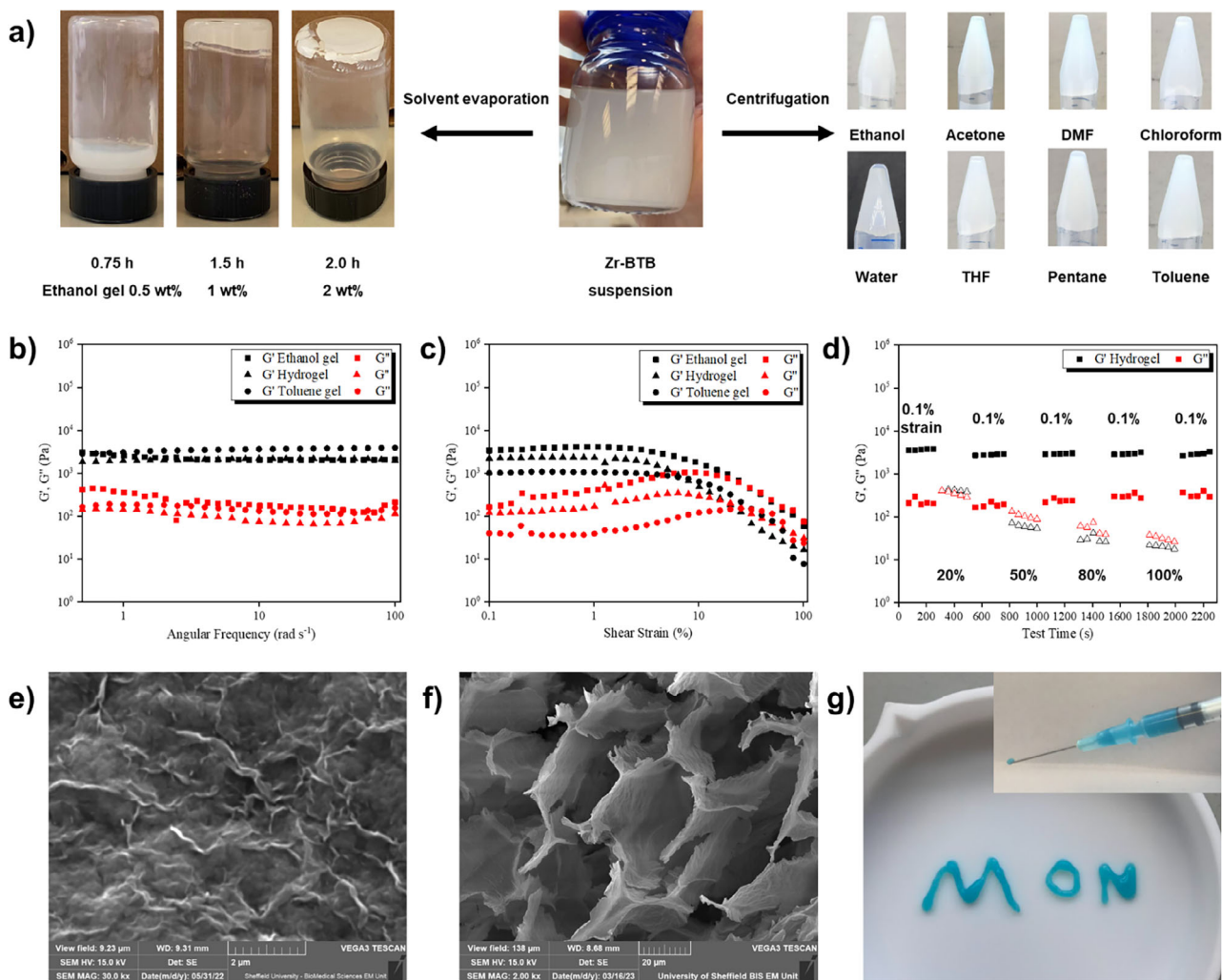


**Figure 2.** a) Preparation of Zr-BTB gels by solvent evaporation and centrifugation. b) Frequency-sweep rheological measurements of the ethanol gel, hydrogel, and toluene gel prepared by centrifugation. This rheological experiment was conducted with a fixed shear strain of 0.1%. c) Strain-sweep rheological measurements of the ethanol gel, hydrogel, and toluene gel prepared by centrifugation. This rheological experiment was conducted with a fixed angular frequency of  $1 \text{ rad s}^{-1}$ . d) Rheological measurements of the hydrogel prepared by centrifugation. This recovery data showed the self-healing behavior of the gel, and this rheological experiment was conducted at different shear strains with a fixed angular frequency of  $1 \text{ rad s}^{-1}$ . e) SEM image of the hydrogel prepared by centrifugation. The sample was dried on the SEM sample disc at room temperature. f) SEM images of Zr-BTB aerogel prepared by freeze-drying of the hydrogel sample. Additional SEM images of the aerogel can be found in Figure S11b–f (Supporting Information). g) Photographs of the hydrogels being loaded into a syringe and extruded through a needle and processed into the word “MON.” The hydrogel was dyed with methylene blue (MnB).

centrifugation at 4500 rpm for just 10 mins. Longer centrifugation times of 1 h were required to form hydrogels, presumably due to the greater stability of the nanosheets in aqueous suspension. Gels could be readily reformed by redispersion of the nanosheets in solvent followed by centrifugation. In order to understand more about the critical gelation concentration, an ethanol suspension of Zr-BTB MONs (10 mL,  $2.5 \text{ mg mL}^{-1}$ ) was heated at  $80^\circ\text{C}$  using a hot plate, and the content of MONs in suspension was checked every 15 mins (Figure 2a; Figure S8, Supporting Information). After 1.5 h of solvent evaporation, the material in the vial changed from a flowing liquid to a non-flowing gel stable with respect to inversion of the vial. After further heating for 0.5 h, the content of MONs in the gel increased from 1 to 2 wt.%, and a shrinkage in the volume of the gel was observed. This

could be attributed to the capillary forces exerted during solvent evaporation.<sup>[47]</sup>

In order to confirm and quantify gel formation, rheological measurements were undertaken to study the viscoelastic properties of the gels. The storage modulus ( $G'$ ) and loss modulus ( $G''$ ) were measured as a function of angular frequency and shear strain for the ethanol gel, hydrogel, and toluene gel prepared by the centrifugation method. At a low shear strain (0.1%),  $G'$  remained approximately one order of magnitude higher than  $G''$  throughout the frequency range (0.5 to  $100 \text{ rad s}^{-1}$ ), confirming the formation of a gel state across all samples (Figure 2b).<sup>[15]</sup>

When the ethanol gel, hydrogel, and toluene gel were subjected to high shear strains (>10%),  $G'$  became lower than  $G''$ , indicating the gel broke down to display predominantly liquid-like

behavior (Figure 2c). Interestingly, rapid recovery of the hydrogel was observed when the shear strain was alternated between 0.1 and 100%, showing its self-healing behavior (Figure 2d).

SEM characterizations of the dried hydrogel (Figure 2e) and ethanol gels (Figures S7, S9, and S10, Supporting Information) showed wrinkled nanosheets that are tens of nanometers thick and several microns in lateral dimensions. In order to minimize structural changes caused by thermal drying, a hydrogel sample was first rapidly frozen into a solid and then freeze-dried to form a self-supporting aerogel (Figure S11a, Supporting Information), which was characterized by SEM. As shown in Figure 2f, the aerogel showed large pores tens of microns in size within a continuous network formed by the overlapping of nanosheets (Figure S11b–f, Supporting Information). These images appear consistent with structures observed for gels formed from inorganic nanosheets such as graphene oxide and MXenes.<sup>[38,48]</sup> A wide variety of mechanisms for gel formation by inorganic nanosheets have been reported in the literature, including repulsion-dominated gels formed by highly charged nanosheets and attraction-dominated systems formed by electrostatic or hydrophobic interactions.<sup>[37,43,49]</sup> Reports of centrifugation induced gel formation appear relatively rare, but we note examples of MXene nanosheets formed in ionic liquids<sup>[48]</sup> and  $Y_2O_3$  in benzyl-alcohol and octylamine mixtures<sup>[50]</sup> and titanate nanosheets formed in water.<sup>[37]</sup>

The zeta potential of dilute suspensions of Zr-BTB nanosheets in water was measured to be 30.6 mV ( $\pm 5.3$  mV), indicating an overall positive charge, consistent with previous literature reports.<sup>[51–54]</sup> The MONs were digested and analyzed by NMR, which showed a lower than expected formate: ligand ratio (1.14:1 rather than 3:1 for the ideal structural formula of  $Zr_6O_4(OH)_4(HCOO)_6(BTB)_2$ ). Zr-carboxylate frameworks are known to be defect-rich;<sup>[55]</sup> often, any vacant metal sites are matched by formate ions, but that does not appear to happen in this case, consistent with the positive surface charge. The magnitude of the zeta potential is usually considered borderline for a stable colloid, which is consistent with high stability observed for the nanosheets under dilute conditions, but also gel formation when concentrated. The nanosheets themselves also contain a wide range of other functional groups, including hydrophobic aromatic linkers and polar metal clusters, which may interact with each other at short distances in accordance with the Derjaguin–Landau–Verwey–Overbeek (DLVO) theory.<sup>[37,56]</sup>

We therefore suggest that at high concentration and so short distances, electrostatic repulsion between positively charged nanosheets must be overcome by favorable van der Waals interactions, causing them to overlap and stack together in a mismatched way to create the sample spanning honey-comb network observed by SEM. The high aspect-ratio and surface area of the nanosheets mean that they have a low percolation threshold, so they can form a continuous network at relatively low concentrations ( $\approx 1.5$  wt.% in this case) when concentrated by centrifugation or evaporation. However, this network must be balanced by strong nanosheet-solvent interactions and repulsive nanosheet-nanosheet interactions, which allow them to trap solvent, prevent collapse of the gels, and allow them to self-heal and redisperse to form stable suspensions of nanosheets. The tunability of MONs makes them ideal candidates for future experimental and computational studies to systematically understand the role of differ-

ent functional groups in giving rise to gel formation and build a more detailed picture of the structure and properties of these gels in different solvents.

### 2.3. Cargo Loading Experiments

MOFs<sup>[57]</sup> and gels<sup>[58]</sup> have been widely used in cargo loading and release applications due to their porous nature and tunable chemistry, but a key limitation of both is the rate at which cargo molecules can be absorbed from solutions. Here, we sought to take advantage of the facile centrifugation method to rapidly load a range of model cargoes into the Zr-BTB gels. Five model cargoes that absorb in the UV-vis region were investigated to understand the effect of size and charge on cargo loading. Trans-anethole (T-Ane) was selected as a small neutral molecule, carbamazepine (CBZ) as a larger neutral molecule, methylene blue (MnB) as a small positive molecule, methyl orange (MO) as a small negative molecule, and brilliant blue G (BBG) as a larger negatively charged molecule.

The cargo loading experiments were conducted by centrifugation of ethanol suspensions containing Zr-BTB MONs and the corresponding cargo molecules. After centrifugation at 4500 rpm for 1 h, the cargo-loaded ethanol gel formed at the bottom of the cuvette (Figure S18a,b, Supporting Information). The concentrations of the cargo solutions before and after the experiment were measured by UV-vis spectroscopy to calculate the percentage loadings, and the results were summarised in Figure 3a and Table S4 (Supporting Information). The concentrations of the two neutral molecules (T-Ane and CBZ) in solutions were almost unchanged before and after the experiments (Figures S19 and S20, Supporting Information), indicating low cargo loadings into the gels. Significantly higher loadings were observed for charged cargo molecules MnB ( $65.6 \pm 1.1\%$ ), MO ( $77.2 \pm 2.4\%$ ), and BBG ( $68.5 \pm 0.2\%$ , Figure 3a; Table S4, Supporting Information). This could be attributed to electrostatic interactions between the charged cargo molecules and the nanosheets. Like other zirconium-based metal-organic frameworks,<sup>[59]</sup> Zr-BTB MONs are defect-rich structures with missing linkers and metal ions creating positively and negatively charged sites, which could bind to the charged cargo molecules (MnB, MO, and BBG, Figure 3b), explaining the increased loading compared to the neutral molecules.

For comparison, a more conventional soaking method was also used, in which the cargo solutions were layered on top of pre-formed Zr-BTB ethanol gels (Figure S24, Supporting Information). As shown in Figure 3a and Table S5 (Supporting Information), the soaking method took  $\approx 72$  h to achieve comparable loadings to the centrifugation method. The cargo loading experiments were also repeated using hydrogels. As shown in Figure S30 (Supporting Information), a uniform loading of the Zr-BTB hydrogel with MnB was achieved when the centrifugation method was used. However, the MnB was not loaded evenly into the Zr-BTB hydrogel by the soaking method (Figure S31, Supporting Information) and instead forms a blue layer only on the top of the gel. This is presumably because in water, MnB adsorbs too strongly to the nanosheets on the surface of the gel, so it is not able to evenly diffuse throughout. Gel formation by centrifugation, therefore, provides a faster and more uniform

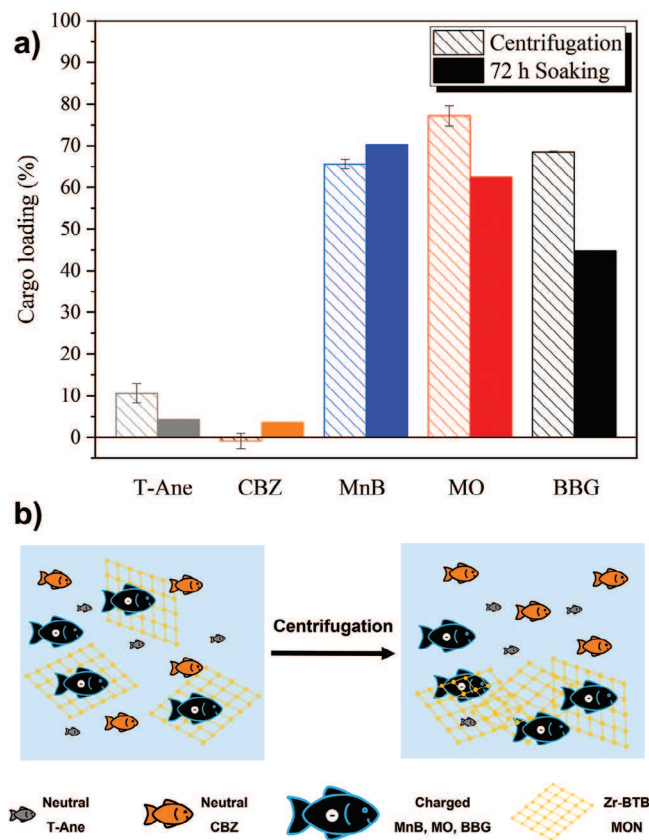


**Figure 3.** a) UV-vis spectroscopy results of the cargo loading experiments, comparing the centrifugation method and the soaking method. For the centrifugation method,  $n = 3$  for error bars. The models of T-Ane, CBZ, MnB, MO, and BBG can be found in Figures S42–S46 (Supporting Information). b) Schematic illustration of the selective loading of cargo molecules into Zr-BTB gels using the centrifugation method. Charged cargo molecules showed significantly higher loadings compared to the neutral ones.

route to load strongly interacting cargo molecules into the Zr-BTB gels by taking advantage of the high surface area of MONs in suspension.

The organogels and hydrogels also showed excellent processability and could be loaded into a syringe and extruded through a needle, allowing them to be processed into complex shapes, such as the word “MON” (Figure 2g; Figure S32, Supporting Information). The hydrogels retained their shape for several hours in solvents such as chloroform, pentane, and DI water. This could be explained by the self-healing behavior of the hydrogel and shows the advantages of the gel state in enabling MONs to be formed into useful shapes. The hydrogel extruded through a needle was also loaded onto the rheometer, and data shown in Figures S16 and S17 (Supporting Information) confirmed its gel state.

#### 2.4. Cargo Release Experiments

The gel state offers solid-like rheology for a material that is largely liquid in composition, making it ideal for the loading and release of small molecules into and out of solution.<sup>[21]</sup> The ability to do this selectively and in a controlled way is key to a wide

range of applications, including water purification<sup>[60]</sup> and the delivery of drugs,<sup>[61]</sup> pesticides, and fertilisers.<sup>[62]</sup> As porous 2D materials, MONs have shown great promise for use in separation applications, including gas separation,<sup>[63]</sup> dye separation<sup>[26]</sup> and desalination.<sup>[32]</sup> Their open structure provides well-defined channels through that can exclude molecules above a certain size.<sup>[64]</sup> Their 2D shape also creates a tortuous path around which larger molecules must pass, interacting with the surface of the nanosheets as they go, allowing for differentiation.<sup>[64]</sup> The nanosheets can be imagined as “fishing nets,” which allow some small molecules “fish” to pass through, large molecules to go around, and charged molecules to get temporarily trapped (Figure 4a). We hypothesised that these mechanisms might also be harnessed within the hierarchically porous gel to enable differential release of molecules depending on their size and charge.

In order to test this hypothesis, fresh ethanol was layered on top of the Zr-BTB ethanol gels loaded with different cargo molecules (Figure S33a,b, Supporting Information), and the cargo concentrations in ethanol above the gel were monitored by UV-vis spectroscopy over time (Figures S34–S38, Supporting Information). As shown in Figure 4b, the T-Ane showed the fastest release rate among the five cargo molecules, its concentration reached equilibrium after 6 h, whereas the concentration of CBZ in ethanol took  $\approx 18$  h to reach equilibrium.

Low cargo loadings and no significant absorption was observed for T-Ane and CBZ in the cargo loading experiments, indicating that there were only weak interactions between the two neutral cargo molecules and the Zr-BTB MONs (Figure 3a). The reported pore size of Zr-BTB in the literature is  $\approx 0.54$  nm,<sup>[65]</sup> larger than the calculated width of T-Ane at 0.43 nm (Figure S42, Supporting Information), but smaller than the width of CBZ at 0.67 nm (Figure S43, Supporting Information). The Stokes-Einstein Gierer-Wirtz Estimation (SEGWE) was used to model the rates of diffusion, taking into account differences in molecular weights. The calculated distance of diffusion for CBZ was  $\approx 1.5$  times as long as that of the T-Ane (Table S6, Supporting Information). These results therefore broadly support our “fish and fishing net” hypothesis (Figure 4a) with T-Ane molecules small enough to be able to pass through the pores of Zr-BTB MONs allowing them to take more direct and shorter diffusion paths, whereas larger CBZ molecules have to pass around the nanosheets, so took more tortuous and longer diffusion paths when they were released from the gels. It is worth noting that this is the opposite trend to the one expected for 3D porous materials, where smaller molecules would be trapped in the pores, leading to longer residence times and slower release rates, as in gel-permeation chromatography (GPC).

The release rates of charged cargo molecules were significantly slower than those of neutral ones. As shown in Figure 4b, the concentration of positively charged MnB levels off after  $\approx 34$  h, almost doubling the release time of CBZ. Moreover, the two negatively charged cargo molecules (MO and BBG) required approximately two weeks to reach their concentration equilibria (Figure 4c). The diffusion path-lengths of the two negatively charged dyes were calculated to be similar despite their size differences (Table S6, Supporting Information). This indicates electrostatic interactions, rather than size differences, dominate in the case of charged cargo molecules. The defect-rich Zr-BTB MONs have an overall positive charge, which is likely to bind

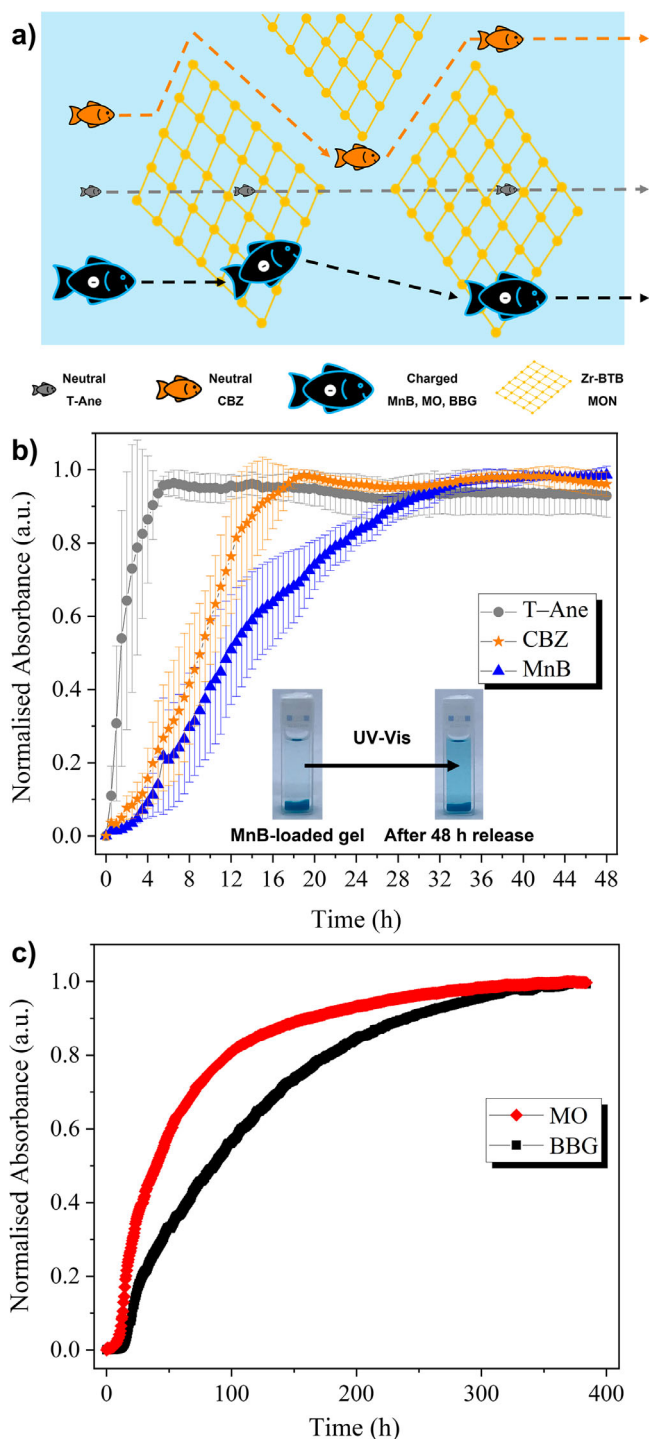


**Figure 4.** a) Schematic illustration of the “fish and fishing net” hypothesis. Small neutral “fish” are able to pass more easily through the pores of Zr-BTB MONs, larger molecules have to take a more tortuous path around the nanosheets, slowing down their release rates. Charged molecules stick to the nanosheets through electrostatic interactions, resulting in even slower release rates. b) UV-vis results of T-Ane, CBZ, and MnB release experiments,  $n = 3$  for error bars. The inset photographs show the MnB-loaded gel before and after the release experiment. c) UV-vis result of MO and BBG release experiments,  $n = 3$  for error bars.

to negatively charged cargo molecules, increasing their absorptions and loadings, but resulting in their slower release rates compared to the neutral ones. Another possibility is that sulfate groups on the negatively charged MO and BBG dyes coordinate reversibly to Zr ions, slowing their release.<sup>[34,66]</sup> Therefore, in the “fish and fishing net” hypothesis (Figure 4a), the much longer release time of charged cargo molecules can be explained by the negatively “charged fishes” sticking to the positively charged “fishing nets.”

### 3. Conclusion

In this work, we showed how suspensions of MONs can be centrifuged to form hierarchically porous gels able to differentially absorb and release molecules based on their size and charge. Monolayer Zr-BTB nanosheets were shown to form both organogels and hydrogels through a facile centrifugation process. Rheological characterisation of these gels for the first time revealed rapid self-healing behavior, which allows them to be passed through a needle and formed into complex shapes. They form stable aerogels following freeze drying, and characterisation by SEM reveals a porous structure formed by overlapping nanosheets. The structure and properties of the Zr-BTB gels are similar to those seen for many graphene oxide nanosheet-based gels, but with the addition of the intrinsic micropores of Zr-BTB MONs alongside the macropores of the gels. Preliminary studies in our own lab have shown that a variety of related Zr- and Hf-tricarboxylate based nanosheets also form gels, and we anticipate that the approach should be broadly applicable to other MONs and related molecular 2D materials.

A key advantage of our centrifugation approach is that it allowed rapid and uniform loading of cargo molecules into the gels by harnessing the high surface area of the nanosheets in suspension. Moreover, molecular cargo was found to diffuse out of the gels at very different rates (from 6 h to  $\approx 2$  weeks), which was attributed to the different diffusion paths available to different molecules depending on their size and charge. In particular, neutral molecules small enough to pass through the pores of Zr-BTB MONs diffused more rapidly out of the gel, whereas larger molecules had to take a more tortuous diffusion path around the nanosheets. This ability to differentiate between molecules based on their molecular size arises from the unique combination of intrinsically porous nanosheets, and the hierarchically porous structure offers new opportunities for the release of multiple drugs or pesticides at different rates depending on the path they can take through the gel.

Overall, this work demonstrates a promising new route for transforming a diverse and highly tuneable class of 2D materials into the gel state. The solid-like rheology of gels offers distinct new opportunities for processing MONs and allowing them to be used heterogeneously to interact with molecules in solution or the gas phase. The porous nature of MONs introduces an additional size-selective path not available to gels based on clays and other non-porous nanosheets. We therefore anticipate that the unique combination of properties offered by MON-based gels will provide exciting new opportunities

within a range of capture, sensing, catalysis, and release applications.

## Supporting Information

Supporting Information is available from the Wiley Online Library or from the author.

## Acknowledgements

Thanks to Christopher J. Hill for the preparation of the aerogel.

## Conflict of Interest

The authors declare no conflict of interest

## Author Contributions

The manuscript was written through the contributions of all authors. All authors have approved the final version of the paper.

## Data Availability Statement

The data that support the findings of this study are available in the supplementary material of this article.

## Keywords

2D materials, controlled release, hydrogel, metal-organic framework nanosheets, organogel

Received: March 24, 2025

Revised: June 18, 2025

Published online:

- [1] Z. Hu, E. M. Mahdi, Y. Peng, Y. Qian, B. Zhang, N. Yan, D. Yuan, J.-C. Tan, D. Zhao, *J. Mater. Chem. A* **2017**, *5*, 8954.
- [2] J. K. Wychowanec, H. Saini, B. Scheibe, D. P. Dubal, A. Schneemann, K. Jayaramulu, *Chem. Soc. Rev.* **2022**, *51*, 9068.
- [3] J. Hou, A. F. Sapnik, T. D. Bennett, *Chem. Sci.* **2020**, *11*, 310.
- [4] K. Sumida, K. Liang, J. Reboul, I. A. Ibarra, S. Furukawa, P. Falcaro, *Chem. Mater.* **2017**, *29*, 2626.
- [5] H. Zhu, X. Yang, E. D. Cranston, S. Zhu, *Adv. Mater.* **2016**, *28*, 7652.
- [6] T. Ishiwata, Y. Furukawa, K. Sugikawa, K. Kokado, K. Sada, *J. Am. Chem. Soc.* **2013**, *135*, 5427.
- [7] Y. Furukawa, T. Ishiwata, K. Sugikawa, K. Kokado, K. Sada, *Angew. Chem., Int. Ed.* **2012**, *51*, 10566.
- [8] E. C. Vermisoglou, P. Jakubec, O. Malina, V. Kupka, A. Schneemann, R. A. Fischer, R. Zboril, K. Jayaramulu, M. Otyepka, *Front. Chem.* **2020**, *8*, 544.
- [9] W. Xia, B. Qiu, D. Xia, R. Zou, *Sci. Rep.* **2013**, *3*, 1935.
- [10] Y. Su, K. I. Otake, J. J. Zheng, S. Horike, S. Kitagawa, C. Gu, *Nature* **2022**, *611*, 289.
- [11] C. Gu, N. Hosono, J. J. Zheng, Y. Sato, S. Kusaka, S. Sakaki, S. Kitagawa, *Science* **2019**, *363*, 387.
- [12] Y. Su, K. I. Otake, J. J. Zheng, P. Wang, Q. Lin, S. Kitagawa, C. Gu, *Nat. Commun.* **2024**, *15*, 2898.
- [13] A. Mahmood, W. Xia, N. Mahmood, Q. Wang, R. Zou, *Sci. Rep.* **2015**, *5*, 10556.
- [14] Y. Ma, A. Li, X. Gao, F. Huang, X. Kuang, P. Yang, J. Yue, B. Tang, *Macromol. Rapid Commun.* **2019**, *40*, 1800862.
- [15] V. Somjit, P. Thinsoongnoen, S. Waiprasoet, T. Pila, P. Pattanasattayavong, S. Horike, K. Kongpatpanich, *ACS Appl. Mater. Interfaces* **2021**, *13*, 30844.
- [16] T. Tian, Z. Zeng, D. Vulpe, M. E. Casco, G. Divitini, P. A. Midgley, J. Silvestre-Albero, J. C. Tan, P. Z. Moghadam, D. Fairen-Jimenez, *Nat. Mater.* **2018**, *17*, 174.
- [17] G. J. H. Lim, Y. Wu, B. B. Shah, J. J. Koh, C. K. Liu, D. Zhao, A. K. Cheetham, J. Wang, J. Ding, *ACS Mater. Lett.* **2019**, *1*, 147.
- [18] S. M. F. Vilela, P. Salcedo-Abraira, L. Micheron, E. L. Solla, P. G. Yot, P. Horcajada, *Chem. Commun.* **2018**, *54*, 13088.
- [19] Z. Wang, S. Furukawa, *Acc. Chem. Res.* **2024**, *57*, 327.
- [20] Z. Wang, A. Ozcan, G. A. Craig, F. Haase, T. Aoyama, D. Poloneeva, K. Horio, M. Higuchi, M. S. Yao, C. M. Doherty, G. Maurin, K. Urayama, A. Bavykina, S. Horike, J. Gascon, R. Semino, S. Furukawa, *J. Am. Chem. Soc.* **2023**, *145*, 14456.
- [21] J. A. Foster, R. M. Parker, A. M. Belenguer, N. Kishi, S. Sutton, C. Abell, J. R. Nitschke, *J. Am. Chem. Soc.* **2015**, *137*, 9722.
- [22] Y. Su, B. Li, Z. Wang, A. Legrand, T. Aoyama, S. Fu, Y. Wu, K. I. Otake, M. Bonn, H. I. Wang, Q. Liao, K. Urayama, S. Kitagawa, L. Huang, S. Furukawa, C. Gu, *J. Am. Chem. Soc.* **2024**, *146*, 15479.
- [23] Y. Su, Z. Wang, A. Legrand, T. Aoyama, N. Ma, W. Wang, K. I. Otake, K. Urayama, S. Horike, S. Kitagawa, S. Furukawa, C. Gu, *J. Am. Chem. Soc.* **2022**, *144*, 6861.
- [24] D. J. Ashworth, J. A. Foster, *J. Mater. Chem. A* **2018**, *6*, 16292.
- [25] J. Nicks, K. Sasitharan, R. R. R. Prasad, D. J. Ashworth, J. A. Foster, *Adv. Funct. Mater.* **2021**, *31*, 2103723.
- [26] H. Ang, L. Hong, *ACS Appl. Mater. Interfaces* **2017**, *9*, 28079.
- [27] Y. Peng, Y. Li, Y. Ban, H. Jin, W. Jiao, X. Liu, W. Yang, *Science* **2014**, *346*, 1356.
- [28] G.-Y. Qiao, S. Yuan, J. Pang, H. Rao, C. T. Lollar, D. Dang, J.-S. Qin, H.-C. Zhou, J. Yu, *Angew. Chem., Int. Ed.* **2020**, *59*, 18224.
- [29] H. Yuan, G. Liu, Z. Qiao, N. Li, P. J. S. Buenconsejo, S. Xi, A. Karmakar, M. Li, H. Cai, S. J. Pennycook, D. Zhao, *Adv. Mater.* **2021**, *33*, 2101257.
- [30] X. Feng, Y. Ren, H. Wang, W. Wu, H. Jiang, *Catal. Sci. Technol.* **2023**, *13*, 7036.
- [31] D. Zhan, Z. Yu, A. Saeed, Q. Hu, N. Zhao, W. Xu, J. Wang, L. Kong, J. Liu, *J. Mater. Chem. C* **2023**, *11*, 10738.
- [32] H. Yuan, K. Li, D. Shi, H. Yang, X. Yu, W. Fan, P. J. S. Buenconsejo, D. Zhao, *Adv. Mater.* **2023**, *35*, 2211859.
- [33] Y. Cheng, S. R. Tavares, C. M. Doherty, Y. Ying, E. Sarnello, G. Maurin, M. R. Hill, T. Li, D. Zhao, *ACS Appl. Mater. Interfaces* **2018**, *10*, 43095.
- [34] X. Feng, Y. Song, W. Lin, *J. Am. Chem. Soc.* **2021**, *143*, 8184.
- [35] D. Parviz, S. A. Shah, M. G. B. Odom, W. Sun, J. L. Lutkenhaus, M. J. Green, *Langmuir* **2018**, *34*, 8550.
- [36] H. Lu, S. Zhang, L. Guo, W. Li, *RSC Adv.* **2017**, *7*, 51008.
- [37] K. Sano, N. Igarashi, Y. Ebina, T. Sasaki, T. Hikima, T. Aida, Y. Ishida, *Nat. Commun.* **2020**, *11*, 6026.
- [38] H. P. Cong, X. C. Ren, P. Wang, S. H. Yu, *ACS Nano* **2012**, *6*, 2693.
- [39] C. Tipa, M. T. Cidade, J. P. Borges, L. C. Costa, J. C. Silva, P. I. P. Soares, *Nanomaterials* **2022**, *12*, 3308.
- [40] F. Zhang, Y. H. Li, J. Y. Li, Z. R. Tang, Y. J. Xu, *Environ. Pollut.* **2019**, *253*, 365.
- [41] G. Gorgolis, C. Galiotis, *2D Mater.* **2017**, *4*, 032001.
- [42] M. Ghadir, W. Chrzanowski, W. H. Lee, R. Rohanzadeh, *RSC Adv.* **2014**, *4*, 35332.
- [43] J. D. Mangadlao, K. J. Lim, C. Danda, M. L. Dalida, R. C. Advincula, *Macromol. Mater. Eng.* **2018**, *303*, 1700314.
- [44] G. O. Lloyd, M.-O. M. Piepenbrock, J. A. Foster, N. Clarke, J. W. Steed, *Soft Matter* **2012**, *8*, 204.

- [45] G. Picci, C. Caltagirone, A. Garau, V. Lippolis, J. Milia, J. W. Steed, *Coord. Chem. Rev.* **2023**, 492, 215225.
- [46] P. R. A. Chivers, D. K. Smith, *Nat. Rev. Mater.* **2019**, 4, 463.
- [47] B. Bueken, N. Van Velthoven, T. Willhammar, T. Stassin, I. Stassen, D. A. Keen, G. V. Baron, J. F. M. Denayer, R. Ameloot, S. Bals, D. De Vos, T. D. Bennett, *Chem. Sci.* **2017**, 8, 3939.
- [48] W. Yu, Y. Yang, Y. Wang, L. Hu, J. Hao, L. Xu, W. Liu, *Nano-Micro Lett.* **2024**, 16, 94.
- [49] T. B. Becher, C. B. Braga, D. L. Bertuzzi, M. D. Ramos, A. Hassan, F. N. Crespilho, C. Ornelas, *Soft Matter* **2019**, 15, 1278.
- [50] W. Cheng, F. Rechberger, M. Niederberger, *ACS Nano* **2016**, 10, 2467.
- [51] Y. Zheng, Y. Liu, H. Li, Z. Yang, W. Wu, J. Zhang, J. Wu, J. Wang, *Adv. Funct. Mater.* **2025**, <https://doi.org/10.1002/adfm.202500151>.
- [52] H. Li, K. Gao, B. Mo, Q. Meng, K. Li, J. Wu, H. Hou, *Dalton Trans.* **2021**, 50, 3348.
- [53] A. C. Wood, E. C. Johnson, R. R. R. Prasad, M. V. Sullivan, N. W. Turner, S. P. Armes, S. S. Staniland, J. A. Foster, *Small* **2024**, <https://doi.org/10.1002/smll.202406339>.
- [54] N. D. Savić, K. Declerck, R. R. R. Prasad, G. Kalandia, J. A. Foster, T. N. Parac-Vogt, *Adv. Funct. Mater.* **2025**, 35, 2504117.
- [55] M. Taddei, R. J. Wakeham, A. Koutsianos, E. Andreoli, A. R. Barron, *Angew. Chem., Int. Ed. Engl.* **2018**, 57, 11706.
- [56] E. J. Verwey, *J. Phys. Colloid Chem.* **1947**, 51, 631.
- [57] H. Molavi, H. Moghimi, R. A. Taheri, *Appl. Organometal. Chem.* **2020**, 34, 5549.
- [58] Q. Wang, S. Li, Z. Wang, H. Liu, C. Li, *J. Appl. Polym. Sci.* **2008**, 111, 1417.
- [59] M. Taddei, R. J. Wakeham, A. Koutsianos, E. Andreoli, A. R. Barron, *Angew. Chem., Int. Ed.* **2018**, 57, 11706.
- [60] Y. Yang, Q. Zhu, X. Peng, J. Sun, C. Li, X. Zhang, H. Zhang, J. Chen, X. Zhou, H. Zeng, Y. Zhang, *Environ. Chem. Lett.* **2022**, 20, 2665.
- [61] J. Li, D. J. Mooney, *Nat. Rev. Mater.* **2016**, 1, 16071.
- [62] R. A. Ramli, *Polym. Chem.* **2019**, 10, 6073.
- [63] Y. Peng, Y. Li, Y. Ban, W. Yang, *Angew. Chem., Int. Ed.* **2017**, 56, 9757.
- [64] Y. Peng, W. Yang, *Adv. Mater. Interfaces* **2019**, 7, 1901514.
- [65] Y. Pu, Z. Yang, V. Wee, Z. Wu, Z. Jiang, D. Zhao, *J. Membr. Sci.* **2022**, 641, 119912.
- [66] R. R. R. Prasad, D. M. Dawson, P. A. Cox, S. E. Ashbrook, P. A. Wright, M. L. Clarke, *Chemistry* **2018**, 24, 15309.